

Estimating the chromospheric magnetic field from a revised NLTE modeling: the case of HR 7428

I. Busá¹★, G. Catanzaro¹, A. Frasca¹, M. Gangi^{2,1}, M. Giarrusso^{2,1}, F. Leone^{2,1},
M. Munari¹, C. Scalia^{2,1}, S. Scuderi¹

¹INAF - Catania Astrophysical Observatory, Via S. Sofia, 78, 95123 - Catania - Italy

²Department of Physics and Astronomy, University of Catania, Via S. Sofia, 78, 95123 - Catania - Italy

Accepted XXX. Received YYY; in original form ZZZ

ABSTRACT

In this work we use the semi-empirical atmospheric modeling method to obtain the chromospheric temperature, pressure, density and magnetic field distribution versus height in the K2 primary component of the RS CVn binary system HR 7428. While temperature, pressure, density are the standard output of the semi-empirical modeling technique, the chromospheric magnetic field estimation versus height comes from considering the possibility of not imposing hydrostatic equilibrium in the semi-empirical computation. The stability of the best non-hydrostatic equilibrium model, implies the presence of an additive (toward the center of the star) pressure, that decrease in strength from the base of the chromosphere toward the outer layers. Interpreting the additive pressure as magnetic pressure we estimated a magnetic field intensity of about 500 gauss at the base of the chromosphere.

Key words: modeling atmosphere, stellar activity, NLTE radiative transfer, chromosphere, magnetic field

1 INTRODUCTION

HR 7428 (= V 1817 Cygni) is a bright (V=6.3) long-period (108.578d) spectroscopic RS CVn binary composed by a K2 II-III star and a main sequence A2 star (Parsons & Ake 1987). The magnetic activity of the system is well known: Ca II H & K emission was first reported by Gratton (1950), by a detailed analysis of photometric observations Hall et al. (1990) were able to detect starspot signatures on the K2 primary star. It is now well established that the stellar atmosphere of cool stars is characterized by that temperature gradient inversion. An inversion explained in the framework of the magnetic activity theories, but not yet definitively understood. Late-type stars, with H- α in emission, show also a fairly stable chromospheric emission outside flares, see. e.g., Byrne et al. (1998). This reinforces the hypothesis that chromospheres are globally in a quasi-stationary state, modulated mainly by the stellar activity cycle, whose temperature-density structure results from the balance between global dissipation of non-radiative energy and radiative cooling (Kalkofen et al. 1998).

Most of what we know about stars and systems of stars is derived from an analysis of their radiation and this knowledge will be secure only as long as the analytical technique is physically reliable. A well tested technique to get information on physical prop-

erties of chromospheric layers of active stars is the NLTE radiative transfer semi-empirical modeling: for different temperature vs height distributions, the NLTE populations for hydrogen are computed, by solving simultaneously the equations of hydrostatic equilibrium, radiative transfer, and statistical equilibrium. The emerging profiles for some chromospheric lines and continua are computed and compared to the observations. Then, the modeling is iterated until a satisfactory match is found. (see, e.g., Vernazza et al. (1981); Fontenla et al. (1993)). These models are built to match the observations in different spectral features, and make no assumption about the physical processes responsible for the heating of the chromosphere, but can be used as constraints for these processes. The obtained models describe the variations of the essential physical parameters, in particular the temperature, pressure and electron density across the outer atmosphere, and give information on its "mean" state, both temporally and spatially.

The most important problem of this approach lies in the uniqueness of the solution. In fact, knowing that a particular atmosphere would emit a line profile like the one we observe for a given star does not imply that the star has indeed this atmospheric structure, since we do not know whether some other atmosphere would produce the same profile. To solve, or at least to reduce, this problem, the modeling has to be based on several spectral features, with different regions of formation. The amount and the kind of diagnostics used to build an atmospheric model is in fact, very

★ E-mail: ebu@oact.inaf.it

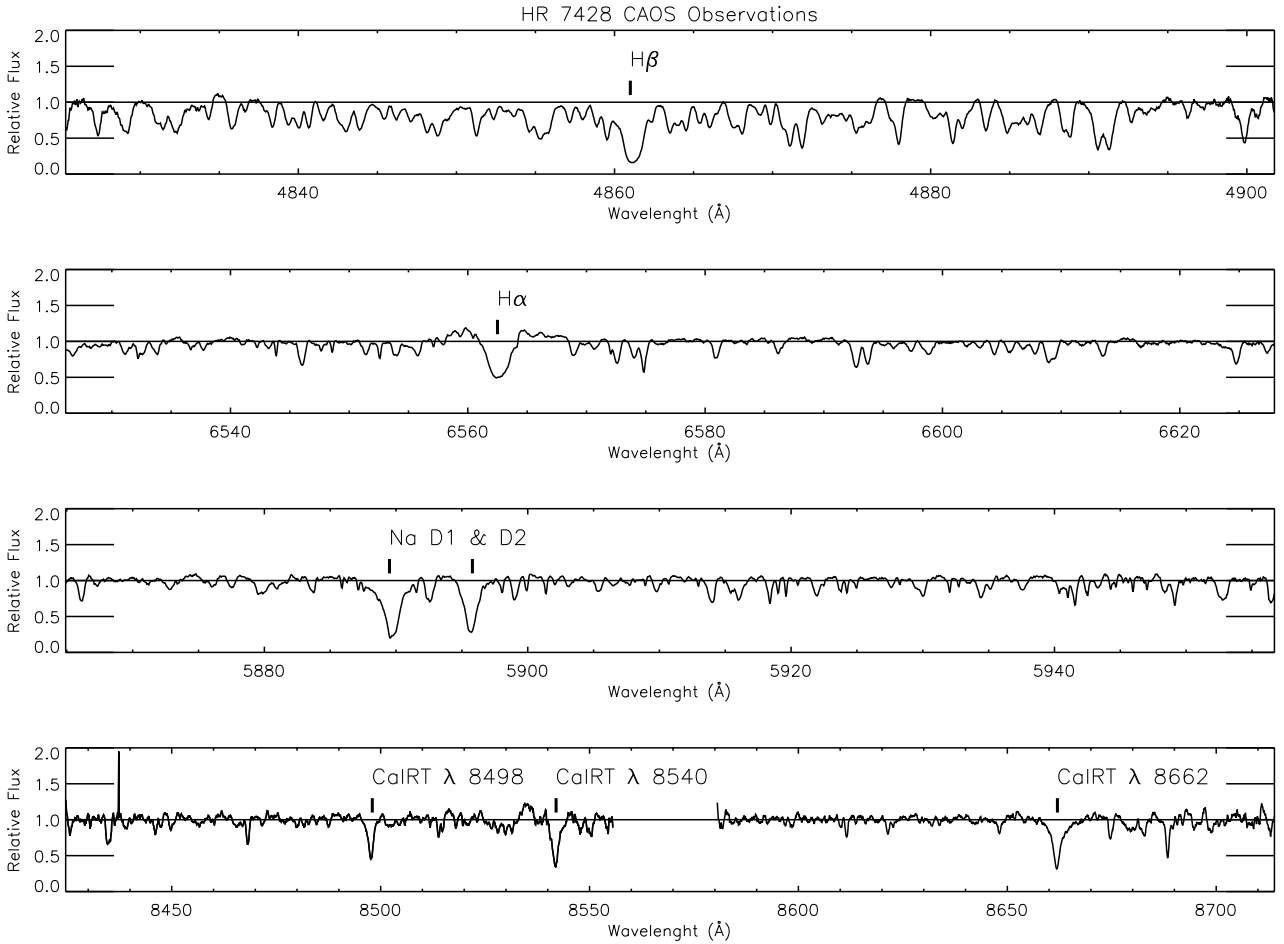


Figure 1. HR7428 normalized spectrum obtained using the new Catania Astrophysical Observatory Spectropolarimeter (CAOS) showing the line profiles of H- β , Na I D, H- α and Ca II IRT lines.

important, by combining several spectral lines that are formed at different but overlapping depths in the atmosphere, we can obtain a more reliable model (Mauas et al. 2006).

Certainly the best known semiempirical model is the one for the average Quiet-Sun, Model C by Vernazza et al. (1981). Semiempirical modeling was successfully applied also to the atmospheres of cool stars. An extensive modeling of dM stars, has been done, starting with the work by Cram & Mullan (1979), Short & Doyle (1998), Mauas & Falchi (1994), and Mauas et al. (1997). Furthermore, a rich history of semiempirical chromospheric modeling has been also carried out for cool giant and supergiant stars (see, e.g., Kelch et al. (1978); Basri et al. (1981); Luttermoser et al. (1994)). In cool stars the application of NLTE semi-empirical chromospheric modelling can be based on optical and ultraviolet (UV) observations. This is because lines such as the H- α Na I D Ca II IRT become dominated by electron-collision excitation processes, which make them effective chromospheric diagnostics (Houdebine 1996). The possibility of using H- α profile as a diagnostic of stellar chromospheres was discussed in detail by Cram & Mullan (1979) and Mullan & Cram (1982) in terms of control of the source function by photons or collisional processes. H- α is observed in active stars in a wide variety of shapes and sizes; when the effective temperature is low enough, the collisional control of the H- α source function becomes possible over a wide range

of chromospheric pressures, and, under this conditions, H- α can be a good chromospheric diagnostic. Mg II h & k UV lines, due to their large opacity, provide excellent diagnostic over a wide range of heights of the outer chromospheric layers (Uitenbroek 1998), and Ca II IRT triplet is a constraint for the shape of the middle chromosphere from the temperature minimum up to the plateau (Andretta et al. 2005).

Here we applied the NLTE semi-empirical chromospheric modelling to the K2 star of HR 7428 binary system basing the analysis on the H- α , H- β , Na I D, Ca II IRT triplet, Mg II h & k lines and UV continuum diagnostics.

2 DATA ACQUISITION AND REDUCTION

H- α Na I D H- β Ca II IRT spectroscopic observations of HR 7428 were carried out at the 91-cm telescope of Catania Astrophysical Observatory, "M. G. Fracastoro" station (Serra La Nave, Mt. Etna, Italy), using the new Catania Astrophysical Observatory Spectropolarimeter (CAOS) which is a fiber fed, high-resolution, cross-dispersed echelle spectrograph (Leone et al. (2016); Spanó et al. (2004), Spanó et al. (2006))

The spectra were obtained in September 2015. Exposure times have been tuned in order to obtain a signal-to-noise ratio of at least

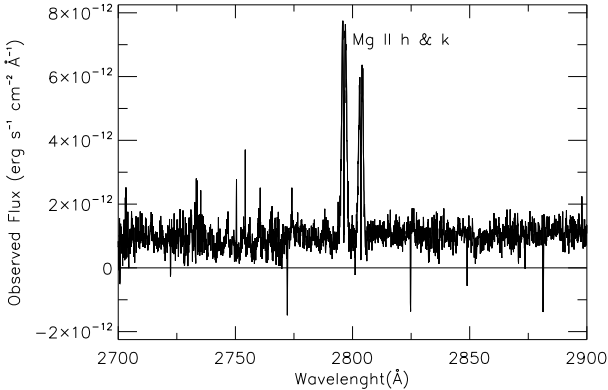


Figure 2. HR7428 high-resolution flux calibrated spectrum in the wavelength of the Mg II line profile obtained by International Ultraviolet Explorer (IUE).

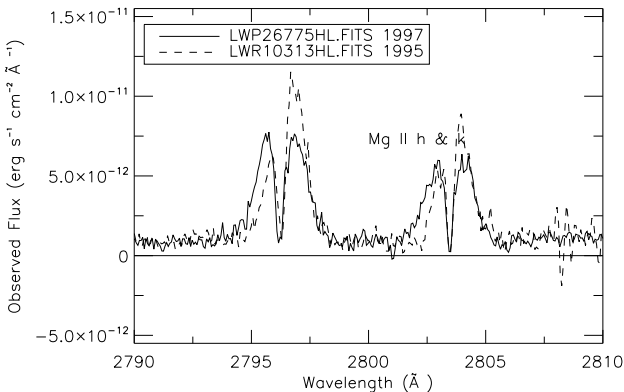


Figure 3. Comparison of two IUE spectra of the system, obtained in different dates: LWP26775HL.FITS obtained in November 1997 and LWR10313HL.FITS obtained in December 1995.

200 in the continuum in the 390-900 nm spectral range, with a resolution of $R = \frac{\lambda}{\Delta\lambda} = 45,000$, as measured from ThAr and telluric lines.

Echelle IRAF packages have been used for data reduction, following the standard steps: bias subtraction, background subtraction, trimming, flat-fielding and scattered light subtraction, extraction for the orders, and wavelength calibration. Several thorium lamp exposures were obtained during each night and then used to provide a wavelength calibration of the observations. Each spectral order was normalized by a polynomial fit to the local continuum. A reduced spectrum, in the wavelength ranges of the line of interest is shown in Fig. 1. In the plotted spectrum the average S/N obtained at the continuum close to H- α is about 200.

Mg II h & k spectroscopic observations have been obtained, in 1997, by the IUE satellite. IUE spectra have been corrected for interstellar extinction. According to the Hipparcos distance

$d = 323 \pm 52$ pc and to the typical value of 1 Mag per kilo-parsec for interstellar extinction we adopted for the computation $A(V) = 0.32$. Assuming the standard reddening law $AV = 3.1 \times E(B-V)$, a color excess $E(B-V) = 0.10$ has been derived. IUE spectra have been de-reddened according to the selective extinction function of Cardelli et al. (1989).

The spectral resolution is about 0.2 \AA for the Mg II region. The IUE flux calibrated HR7428 spectrum, is shown in Fig. 2.

Unfortunately, we have no simultaneous UV and optical observations. Therefore we have to take into account the activity-variability that could affect the HR7428 system, due to different levels of the stellar activity and/or different distribution of the active regions on the visible surface, in different times. In order to have an estimate of how much UV data are affected by activity-variability we have compared two IUE spectra of the system, obtained in different dates: LWP26775HL.FITS obtained in November 1997 and LWR10313HL.FITS obtained in December 1995 (see Fig. 3 where the two Mg II h & k IUE spectra are shown with a shift in wavelength in order to overlap.) $1.060 \times 10^{-12} \pm 1 \times 10^{-15}$ We find that we can neglect the long term variability as far as the UV continuum is concerned, the two spectra show in fact the same continuum mean value (Mg II Continuum Flux(1995) = $1.06 \times 10^{-12} \pm 1 \times 10^{-14} \text{ erg cm}^{-2} \text{ s}^{-1}$, Mg II Continuum Flux(1997) = $1.060 \times 10^{-12} \pm 7 \times 10^{-15} \text{ erg cm}^{-2} \text{ s}^{-1}$). As far as the Mg II h & k line profiles are concerned, we measure approximately equivalent observed fluxes at Earth ($Flux_{Mg II h \& k}(1995) = 3.33 \times 10^{-11} \pm 3 \times 10^{-13} \text{ erg cm}^{-2} \text{ s}^{-1}$, $Flux_{Mg II h \& k}(1997) = 3.20 \times 10^{-11} \pm 3 \times 10^{-13} \text{ erg cm}^{-2} \text{ s}^{-1}$), but the profile shape is quite different as shown in Fig. 3, most probably indicating a different distribution of active regions in different times, that we cannot take into account. Therefore an higher weight will be done to the best fit of the UV continuum with respect to the Mg II h & k line profile.

3 COMPUTATIONAL METHOD

Historically, K2 giants were classified as "non-coronal" stars, however, in the late 1990s, evidence for transition region emission was detected for Arcturus (K2 III) and Aldebaran (K5 III) (Ayes et al. 2003) and for other representative "non-coronal" red giants (see, e.g., Ayes et al. (1997); Robinson et al. (1998)) Therefore, here, the atmospheric model of the K2 primary magnetic active component has been built computing a photospheric model, a chromospheric model and a transition region model and joining the three together; we assume a plane-parallel geometry in our modeling efforts.

3.1 Photospheric Model

Taking into account the Marino et al. (2001) physical parameters (see Table 1) we selected from the Castelli LTE synthetic spectra database (<http://www.oact.inaf.it/castelli/castelli/grids.html>), a spectrum with parameters $\log g \approx 2.0$, $T_{\text{eff}} \approx 4400 \text{ K}$ and solar metallicity that describes the photospheric contribution of the K2 primary component, and a spectrum with parameters $\log g \approx 4.0$, $T_{\text{eff}} \approx 9000 \text{ K}$ and solar metallicity that describes the flux contribution of the A2 secondary component of the binary system HR 7428.

In Fig. 4 the fluxes at Earth of the two LTE models are shown together with their sum. The original fluxes have been converted to flux at Earth by the conversion factor R^2/d^2 that has been calculated for the K and A star according to the parameters given in Tab.1. From the plot we conclude that, for NLTE radiative transfer calculations

Table 1. HR 7428 K2II-III and A2 components (Marino et al. 2001).

Element	Primary (cooler K2II-III)	Secondary (hotter A2)
R	$40.0 \pm 6.5 R_{\odot}$	$2.25 \pm 0.5 R_{\odot}$
T_{eff}	$4400 \text{ K} \pm 150 \text{ K}$	$9000 \text{ K} \pm 200 \text{ K}$
$\log g$	2.0 ± 0.5	4.0 ± 0.5

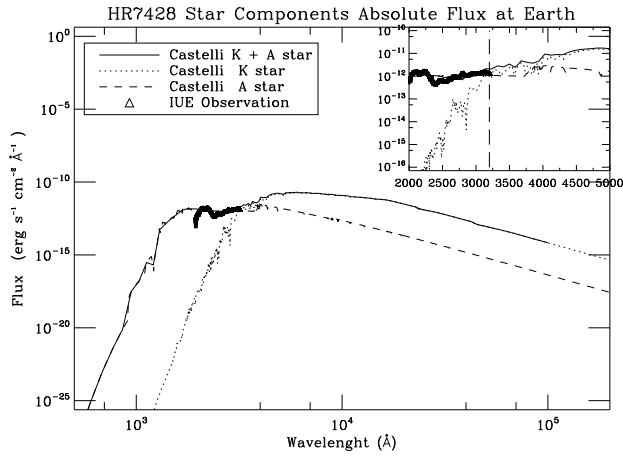


Figure 4. HR7428 Castelli LTE synthetic photospheric fluxes at Earth for the K star (dotted line) and A star (dashed line) where the conversion factor R^2/d^2 has been calculated for the K and A stars according to the parameters given in Tab.1. The plot zoom around 2000-5000 Å shows that before $\lambda = 3200$ Å the A star dominates the continuum emission, while for wavelength greater than $\lambda = 3200$ Å we can neglect the A star contribution, the continuum is in fact dominated by the K star.

of the H- β , Na I D, H- α , Ca II IRT triplet profiles of the binary system, we can neglect the A2 star contribution. In fact, from Fig. 4 we can see that for wavelength longer than 3200 Å, the continuum flux of the binary system is dominated by the K star. This is in agreement with Marino et al. (2001) that find the A2 star contribution to the total flux in the H- α region is only 4%. On the other hand, in order to calculate the NLTE Mg II h & k (wavelength lower than 3200 Å) HR 7428 line profile, we have to take into account the A2 star contribution. In the Mg II h & k spectral range in fact (triangles show the observed IUE Mg II h & k), the observed continuum is dominated by the A star contribution.

Therefore, we computed the A2 secondary component atmospheric model by the ATLAS9 code (Kurucz 1993) using the parameters $\log g=4.0$, $T_{\text{eff}}=9000$ K, $[A/H]=0.0$.

The atmospheric model of the K2 primary magnetic active component has been built computing separately a photospheric model, a chromospheric model and a transition region model and joining the three together.

The K2 photospheric model was computed using the ATLAS9 code and the parameters $\log g=2.0$, $T_{\text{eff}}=4400$ K, $[A/H]=0.0$ for the K2 primary component.

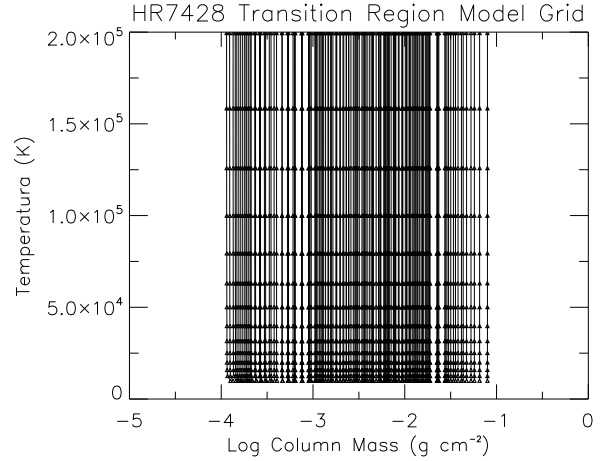


Figure 5. Grid of transition region models used for the study of HR7428 atmosphere. The grid has been built as described in the text.

3.2 Transition Region Model

A first estimation of a plane-parallel model for the lower transition region of the HR 7428 K2 primary component, has been built using the method of the Volumetric Emission Measure. The use of Emission Measure techniques to construct transition region models is well established (see for example Jordan & Brown (1981), Harper (1992)), the flux at the star, for lines forming at temperature $T_e \approx 10^5$ K is in fact dominated by collisions. This results in emission lines that are optically thin and with a contribution function sharply peaked in temperature, that is, typically formed over a temperature range of $\Delta \log T_e = 0.30$.

The above conditions allow to determine the temperature gradient as a function of the averaged Emission Measure over $\Delta \log T_e = 0.30$ that we indicate as $EM_{0.3}$.

By imposing hydrostatic equilibrium, including turbulent pressure, the transition region model can be obtained combining the temperature gradient as a function of $EM_{0.3}$ and the pressure variation from the equation of hydrostatic equilibrium (see e.g., Harper (1992)).

The expression for the temperature gradient combined with the equation of hydrostatic equilibrium gives the relationship:

$$P_{\text{Tot}}^2(T_2) - P_{\text{Tot}}^2(T_1) = 2 \times 1.4^2 m_p g k \times \times T_1^2 EM_{0.3} \times (1 + 1.1x) \frac{1.4x m_p v_{\text{turb}}^2 EM_{0.3}}{2kT} dT \quad (1)$$

where m_p is the H mass, k is the Boltzmann constant, v_{turb} is the turbulent velocity and $x \equiv N_H N_e$.

The Eq. 1 together with an estimate of electron density and turbulent velocity in a layer, allows to find the pressure as a function of temperature for the TR model. The total particle density (N_{tot}), gas pressure (P_G), turbulence pressure (P_{turb}) and electron density (N_e) are then obtained according to the following relations

$$\begin{aligned} N_{\text{tot}} &= \sqrt{P_{\text{Tot}}} (k T + 0.5 m_p v_{\text{turb}}^2) \\ P_G &= N_{\text{tot}} k T \\ P_{\text{turb}} &= 0.5 N_{\text{tot}} m_p \mu v_{\text{turb}}^2 \\ N_e &= N_{\text{tot}} / (1 + 1.1x) \end{aligned} \quad (2)$$

where $\mu \equiv \frac{1.4 N_H N_e}{(1 + 1.1 N_H N_e)}$ is the molecular weight.

We used the equations above in order to build plane-parallel

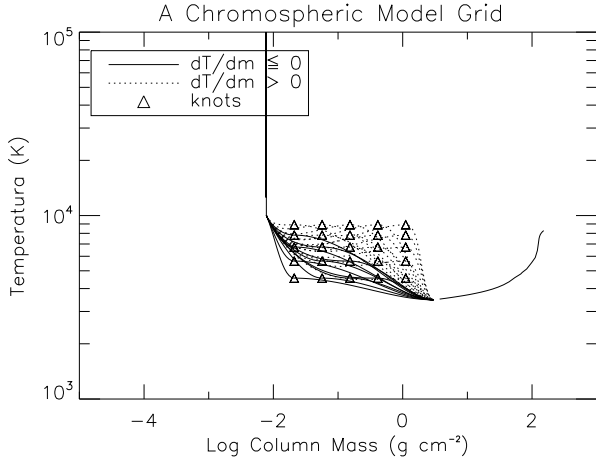


Figure 6. Grid of chromospheric structures obtained by spline interpolation between a fixed Transition Region model and a fixed Photospheric model, using as free parameters a grid of 25 knots point. The figure shows in dotted lines the models that do not satisfy the negative gradient condition $dT/dm \leq 0$.

models for the lower transition region of the HR 7428 K2 primary component.

In order to have an estimate of Emission Measures for the HR 7428 binary system, we used, the values of Volumetric Emission Measure (VEM) vs T_{eff} measured by Griffiths & Jordan (1998) for another RS CVn system, HR 1099 primary component ($R_{HR1099K1IV} = 3.9 R_{\odot}$), opportunely scaling them, in order to take into account the bigger radius ($R_{K2} = 40 R_{\odot}$) of HR 7428 K2 star, according the formula $EM_{0.3} = VEM 4\pi R^2$ (Brown et al. 1991) and the parameters of Table, 1.

From the estimated $EM_{0.3}$ values, a grid of 160 transition region models, shown in Fig. 5 has been built by means of equations 1 and 2 using a grid of 23 values of electron density at the fixed temperature $T_e = 50000$ K obtained scaling of a factor from 0.5 up to 30 the values of electron density at 50,000 K measured in HR 1099 ($N_e = 5 \times 10^{11} \text{cm}^{-3}$). For each of these 23 electron density values, a grid of seven values of the turbulent velocity in the layer with $T_0 = 10^4$ K, $v_{\text{turb}}(T_0 \equiv 10^4 \text{K}) = 10, 20, 30, 40, 50, 60, 70 \text{ km s}^{-1}$ has been considered for the calculation of turbulent velocity distribution according the empirical law by Griffiths & Jordan (1998) $v_{\text{turb}}(T) = v_{\text{turb}}(T_0) \times (TT_0)^{1.4}$ between $\log T = 4.0$ and $\log T = 5.3$.

These transition region models provide the upper boundaries for the radiative transfer calculations of the chromospheric models, while the adopted photospheric model provides the lower boundaries of the chromospheric models.

3.3 Chromospheric Model

The term ‘chromosphere’ indicates the region above a stellar photosphere where non-radiative heating processes (either magnetic or acoustic) become important in the energy balance and where hydrogen is partially ionized. Since hydrogen is nearly completely ionized when temperatures reach 20,000-30,000 K, we consider this the top of chromosphere. Once hydrogen is nearly completely ionized, mechanical heating produces a steep thermal gradient because there is no cooling channel as effective as hydrogen, and Ca II, Mg II have disappeared before hydrogen is ionized (Linsky et al. 2001).

Chromospheres lies in the difficult regimes of non-LTE and non-ionization equilibrium. While photosphere can be calculated in detail when having $\log g$, $[A/H]$ and T_{eff} , and transition region can be constrained by observations because lines form in optically thin conditions as seen before, for the chromospheric layers we have no constraints, lines are optically thick, and the chromospheric model has to be based upon spectral diagnostic methods by means of semi-empirical modeling technique, that is changing an hypothetic model iteratively, in order to match as many as possible observations that form in the chromospheric layers. We can only suppose that the temperature increases with a smooth thermal gradient because, the non-radiative sources heats the plasma producing bright emission in the H- α , Ca II IRT, Mg II h & k which together are the dominant cooling channels of the chromosphere. In the Sun the chromosphere goes from ≈ 600 km and ≈ 2000 km above the photosphere and is characterized by temperature gradient sign change, where temperature smoothly grow from ≈ 4500 K up to ≈ 15000 K over which the gas density changes by several orders of magnitude due to a sharp decrease of turbulent pressure while the electron density only smoothly decrease.

The solar chromosphere has been described for the first time by Vernazza et al. (1973) by means of a one-component model of the solar atmosphere, including in that model the photosphere, chromosphere and transition zone, and then in detail, by Fontenla et al. (1999), who using the PANDORA NLTE radiative transfer code determine semiempirical models for seven semiempirical models for sunspots, plages, network, and quiet atmosphere constructed to reproduce observed emergent intensities and profiles at wavelengths from the UV to radio wavelengths.

While Vernazza et al. (1973) determine the chromospheric model of the Sun by adjusting the temperature as a function of height to that distribution that gives best agreement between synthesized and observed line spectra, here we have built a wide grid of chromospheric models from which to look for the best model by means of a χ^2 minimization selection method.

In particular, for each one of the 160 transition region model and for each of nine values of T_{min} in the range between ~ 2800 K and 4200 K that we have chosen with a step of less than 200 K as points where to cut the photospheric Kurucz model, a grid of 25 chromospheric models are generated by a smooth spline interpolation between the photosphere and the transition region using as free parameters a grid of 5×5 interpolation knots, (see Fig. 6, where the grid of 25 chromospheric models is shown for a fixed TR model and a fixed minimum of photospheric model T_{min} . We impose the chromospheric structures to have a monotonic temperature dependence on Column Mass ($dT/dm \leq 0$). Fig. 6 shows how the temperature gradient constraint, strongly cuts the number of useful model of the grid, for example in the 25 model grid of the figure, only eight models satisfy the gradient constraint and can be used in the analysis.

The total grid of models includes $160 \times 9 \times 25 = 36225$ models, and only 15691 satisfy the $dT/dm \leq 0$ constraint and have been considered in the NLTE radiative transfer.

3.4 Computation: applying or not hydrostatic equilibrium equations

The coupled equations of radiative transfer and statistical equilibrium were solved using the version 2.2 of the code *Multi* (Carlsson 1986), for the H, Ca, Na, Mg atomic models. The H atomic model incorporates 16 states of H, with 84 $b-b$ and 9 $b-f$ transitions. The Ca atomic model incorporates 8 states of Ca I, the lowest 5 states

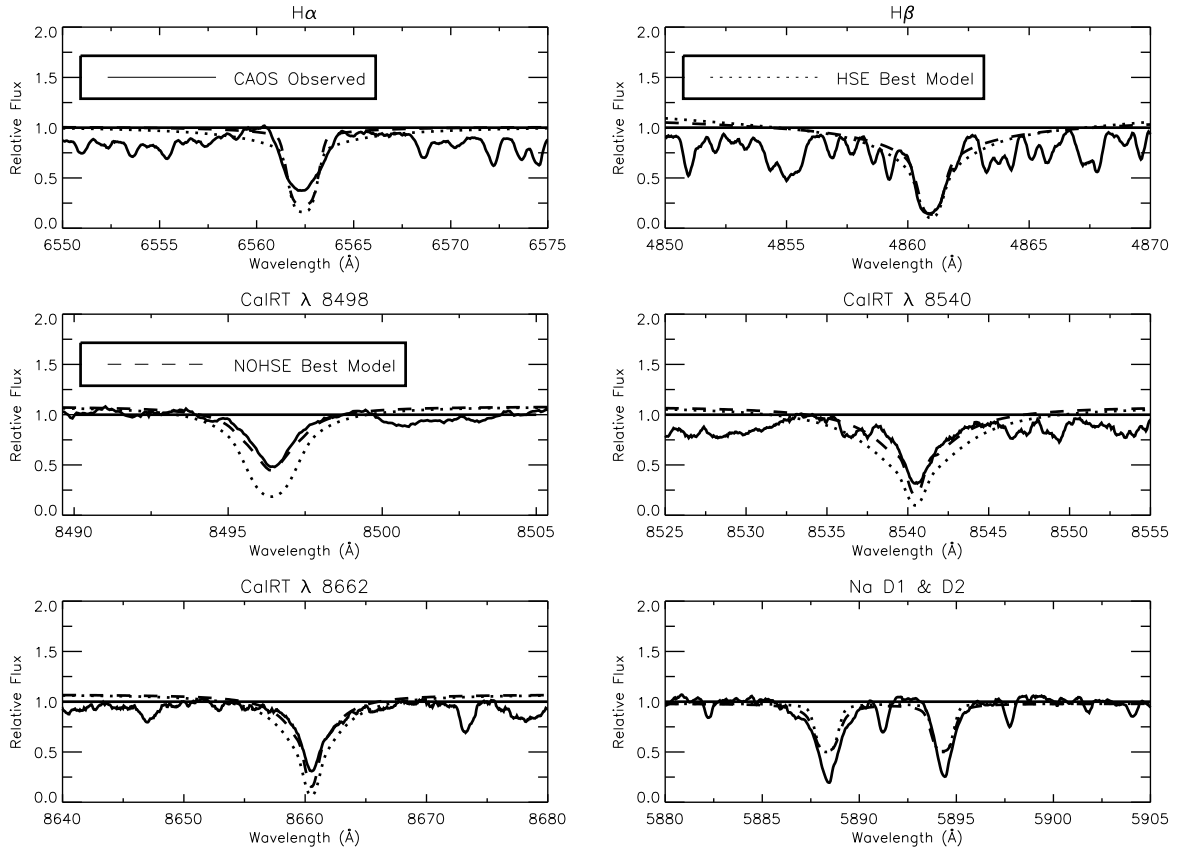


Figure 7. NLTE H- α , H- β , Ca II IRT, Na I D normalized profiles computed for the best *HSE* (dotted line) and the best *NOHSE* (dashed line) models compared with observations.

of Ca II and the ground state of Ca III, 9 *b-b* and 13 *b-f* transitions are treated in detail. The Mg II atomic model is made of 3 states Mg I, the lowest 6 states of Mg II and the ground state of Mg III, 9 *b-b* and 9 *b-f* transitions are treated in detail. The Na atomic model incorporates 12 levels: 11 levels of Na I and the ground state of Na II and 29 *b-b* and 11 *b-f* transitions are treated in detail. The opacity package included in the code takes into account free-free opacity, Rayleigh scattering, and bound-free transitions from hydrogen and metals. We included the line blanketing contribution to the opacity using the method described in [Busá et al. \(2001\)](#).

As a first step we imposed hydrostatic equilibrium to the hydrogen, that is, we calculated the hydrogen radiative transfer and the equation of hydrostatic equilibrium consistently. In detail, starting with the LTE hydrogen populations for the electron pressure and density calculation, hydrogen is iterated to convergence. Then hydrostatic equilibrium $dP_{Tot} = \rho g dh$ is solved and electron pressure and hydrogen populations are updated, the loop continues until we obtain a convergence. The electron density is then used to solve the Ca, Mg, and Na radiative transfer and statistical equilibrium equations. The population densities obtained from the H calculation are used to obtain the background NLTE source function in the Ca, Mg, and Na calculations. This computation modifies the initial grid because a new column of electron density is obtained, we find that only 2052 models converge to a solution and we call them *HSE* models.

We also considered not imposing hydrostatic equilibrium that means fixing the electron densities to the ones of the original grid.

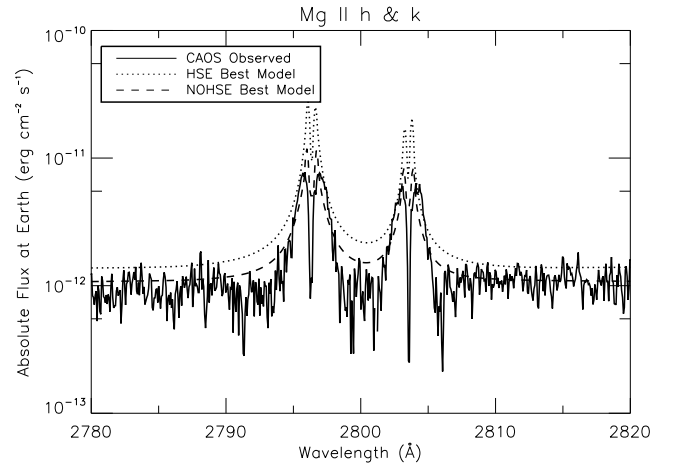


Figure 8. Mg II h & k absolute flux profiles computed from the best *HSE* and the best *NOHSE* atmospheric models compared with the IUE observation.

In this case we consider all the 15691 models that only satisfy the $dT/dm \leq 0$ constraint and we call these models, *NOHSE* models.

Even if an atmospheric model in non-hydrostatic equilibrium is not realistic and should be rejected, here we assume the *NOHSE* models as good as the *HSE* ones. Of course hydrostatic equilibrium has to happen in the star, but, because we are not taking into

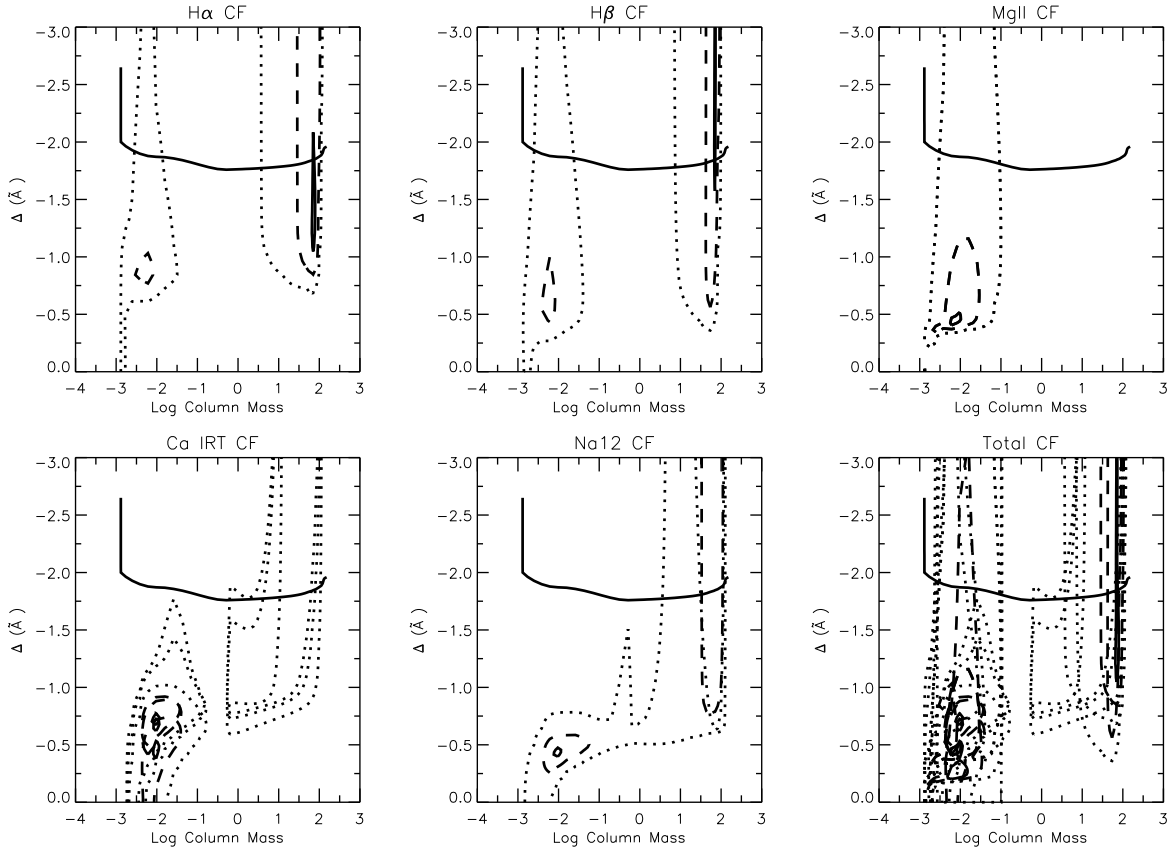


Figure 9. Contribution functions of the H- α , H- β , Mg II h & k, Ca II IRT, Na I D lines for the best *NOHSE* model. The maximum of the contribution function is set equal to one. The contour plot indicates the fractions 0.9 (solid), 0.3 (dashed) 0.01 (dotted). The atmospheric model is plotted as a solid line in each *CF* plot. The last plot, where all lines contribution functions are plotted together, indicates that our selected diagnostics mainly constraint the whole atmosphere (H- α and H- β wings), and chromosphere (all the lines) up to the transition region (Mg II h & k cores) giving strength to our semiempirical modeling.

account all the pressure contributions to the total pressure, therefore we can assure that also the *HSE* models should be rejected, or, at least can be, good or not, just like the *NOHSE* models. In a sense, we can assume that, imposing *HSE*, the resulting model is not in hydrostatic equilibrium if a contribution to the pressure is missing in the $dP_{Tot} = \rho g dh$ equation. And this is the case of cool active stars. We know in fact that the atmospheres of active stars are permeated by magnetic fields that emerge from deeper layers. With increasing height we might expect the structure to be more greatly influenced by magnetic fields, since the energy density of the magnetic fields should fall off more slowly than the energy density of the gas (this is the case of solar atmosphere where $\beta = 8\pi NKT_e|B|^2$ is ≥ 1 in photosphere and $\ll 1$ in transition region layers). Therefore, magnetic pressure should be added in the computation of the total pressure and is not. This lack together with the lack of any other possible contribution not yet identified, let us to say that the electron densities and the hydrogen populations obtained from imposing *HSE* differ from the ones we would have obtained introducing a magnetic field contribution. This approach takes into account the possibility that some pressure contributions are neglected and becomes a method to derive an estimate of the lacking pressure component. In such an approach we use the electron density as a free parameter, looking for the electron density distribution that best fit the data. We accept as best solution, also a distribution whose total pressure is not balancing the gravity, accepting the

hypothesis that a new pressure component could be considered for achieving the equilibrium.

Furthermore, also different approaches in the treatment of line blanketing, produces different N_e vs temperature. It is well known in fact, that the source function of a line can be strongly coupled to radiation fields even at very different wavelengths, via radiative rates determining the statistical equilibrium of the species producing the line.

If we would find as the best model reproducing our data, an *HSE* model, this would mean that magnetic or other contributions to the total pressure are negligible in the whole upper atmosphere of the K2 HR 7428 star.

In the case where a *NOHSE* model should best reproduce the observations this would implies that other pressure contributions are important in the outer atmosphere of our star and we can then infer information on these additive contributions to the total pressure.

Therefore both the *HSE* grid of 2052 models and the initial grid of 15691 model have been considered in the radiative transfer calculations for H, Na, Ca and Mg. For each grid, the models that converge to solution for all the atoms have been taken into account for the comparison with the observed spectrum.

The computed profiles of H- α , H- β , Ca II IRT, Na I D, have been convolved with a rotational profile with $v \sin i = 17$

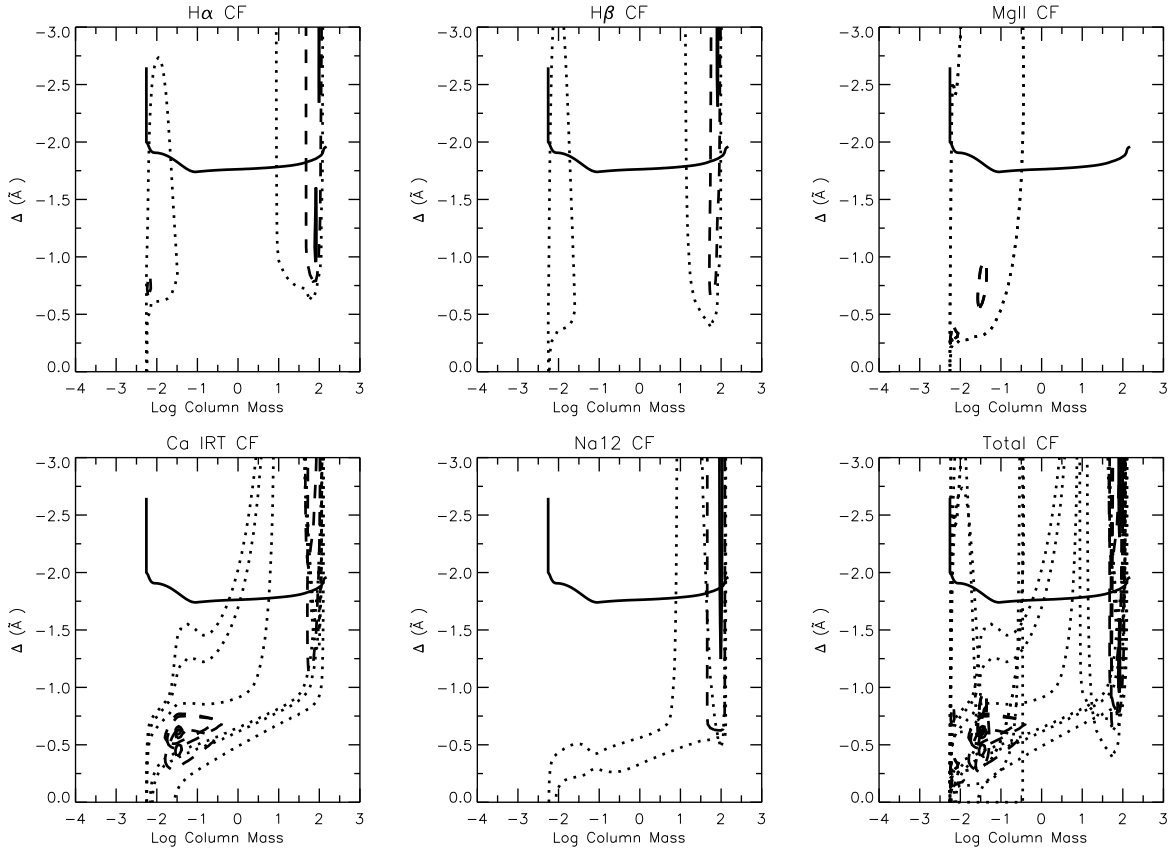


Figure 10. Contribution functions of the H- α , H- β , Mg II h & k, Ca IRT, Na I D lines for the best *HSE* model. Like for the *NOHSE* model (see Fig. 9 also for the *HSE* model the outer atmosphere is enough constrained by our diagnostics.)

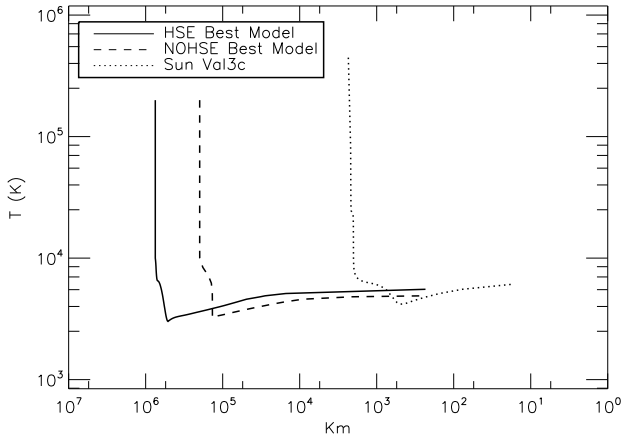


Figure 11. Best atmospheric *HSE* and *NOHSE* models for the mean K2 primary component of the RSCVn system HR 7428 compared with the Solar Val 3c model. The plot describes the distribution of temperature versus height. Height is given in kilometers measured above a zero point where $\tau_{5000} = 1$.

km s⁻¹ (Marino et al. 2001) and an instrumental profile with $R = \frac{\lambda}{\Delta\lambda} = 45,000$, normalized and then compared with observations.

The computed profiles of Mg II h & k have been obtained by the weighted sum of the K2 star profile and the A2 star profile and

weighted for the d^2R^2 factor. Wavelength shifts to account for orbital velocities, are applied to synthetic spectra.

4 COMPARISON WITH OBSERVATIONS: THE BEST MODEL

We used a χ^2 minimization procedure for the selection of the model that best describes the mean outer atmosphere of HR 7428. For each line the χ^2 between each observed and the synthetic line profile has been performed interpolating to the same wavelength grid the two profiles and choosing opportunely the wavelength range for the χ^2 determination. Therefore, for each model, the whole set of observed lines has been compared with the corresponding synthetic lines and a global χ^2_{Tot} for each model has been calculated as the average of the χ^2 obtained for the single line profiles, a 0.5 weight has been applied to the Mg II h & k lines χ^2 in order to take into account the activity-variability as seen in Section 2. We defined a selection box formed of those models which give a χ^2 less than a fixed value for all used lines and UV continuum, the best model is then selected as the one of the box with the lowest χ^2_{Tot} .

We find that the best *NOHSE* model has a $\chi^2_{Tot} = 1.22$ while the best *HSE* model has a $\chi^2_{Tot} = 2.60$. This result lets conclude that the *NOHSE* best model distribution of temperature, gas pressure, electron and population densities versus height is the best description of the mean outer atmosphere of the K2 star of the binary system HR7428.

We will describe here both the two *HSE* and *NOHSE* best

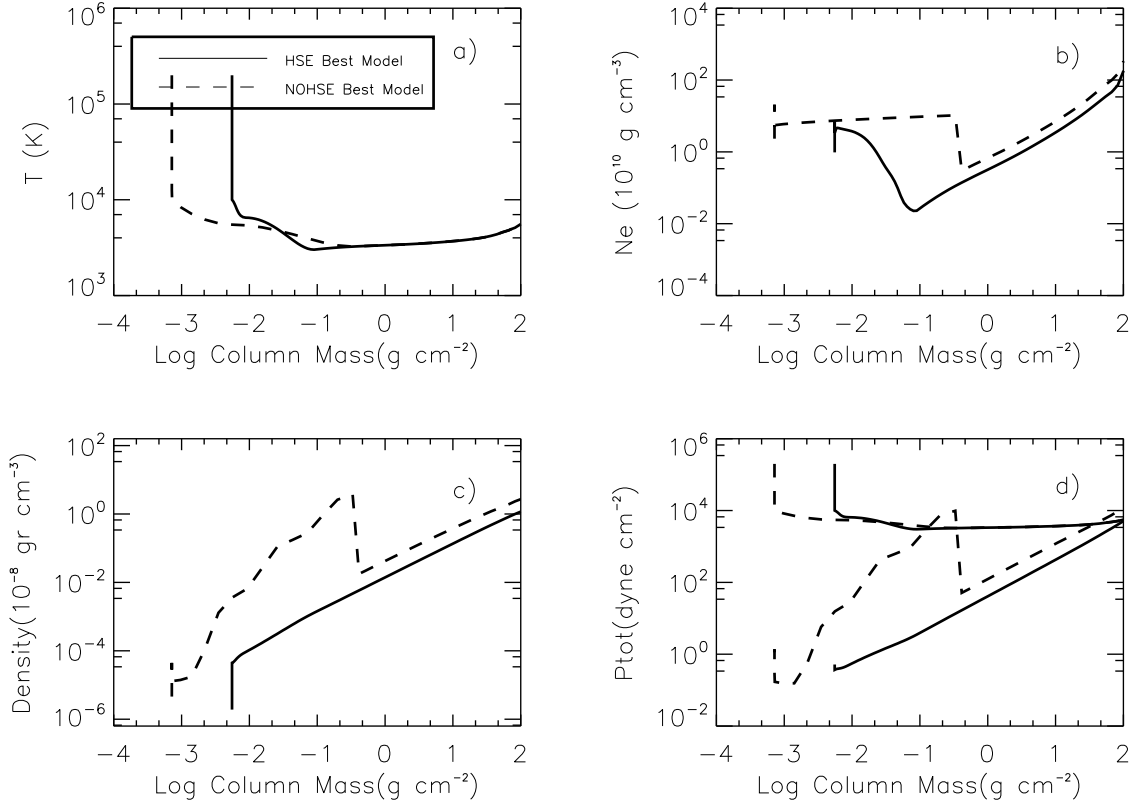


Figure 12. Temperature, electron density, density mass and pressure versus Column Mass for the best *HSE* and *NOHSE* models of the K2 primary component of the RS CVn system HR 7428. In the last plot, the two best models are shown for references.

models as possible representations of the mean outer atmosphere of the K2 star.

The best χ^2_{Tot} of the *NOHSE* model with respect to the *HSE* one is clearly understable from Fig. 7 where the H- α , H- β , Ca II IRT, Na I D synthetic profiles computed for the best *HSE* (dotted line) and the best *NOHSE* (dashed line) models are shown and compared with the observed profiles.

The *NOHSE* model gives Na I D lines somewhat less deep than the observed profile and an H- α profile a bit deeper than the observed one. Nevertheless, the *NOHSE* model reproduce much better than the *HSE* both the Ca II IRT line profiles as well as the H- β profile, furthermore, the also the *HSE* model gives Na I D lines less deep and H- α deeper than the observed one.

The *NOHSE* model gives also a better fit of the Mg II h & k lines as can be seen from Fig. 8 where the IUE observed flux at Earth of the Mg II h & k is compared with the synthetic profiles obtained from the *HSE* (dotted line) and the *NOHSE* (dashed line) best models. We can see how the *NOHSE* best model better reproduce both the continuum emission and the Mg II h & k line profiles. The discrepancy in the peak region of the h and k profiles is compatible with the activity-variability or also to the unresolved ISM absorption line that has not been taken into account in the synthetic lines computation.

Fig. 9 and Fig. 10 show the line contribution functions (*CF*) to the emergent radiation (*CF*) as defined by Achmad et al. (1991), of the synthesized lines in the case of *NOHSE* and *HSE* respectively. The plots mainly indicates the region of formation of the different part of each line, having on the x axis the $\Delta\lambda$ from the center of the

line and on the y axis the Column Mass that corresponds to an the atmospheric layer. In order to make this more clear we overplotted the atmospheric model as a continuous line in each *CF* plot. In the case of Na I D, Mg II h & k and Ca II IRT, the *CFs* of the multiple lines are overplotted together.

We can see that both in the *NOHSE* and in the *HSE* atmospheres, the line formation is very similar.

We find that the base of the transition region is quite well constrained by the H- α and Mg II h & k cores. Also the central part of the Na I D, H- β and Ca II IRT cores are affected by the transition region conditions. Mg II h & k lines, except for the core, form entirely in the chromosphere which is also constrained by the Ca II IRT lines. The line wings of all the used lines, except for Mg II h & k wings, form in the atmospheric region that goes from the photosphere up to the temperature minimum region. The last plot on the right, in Fig. 9 and Fig. 10 shows the overplot of all the lines *CF* and puts in evidence how the used diagnostics enough constrain the whole atmosphere, giving strength to the method and to the atmospheric model derived for the K2 star of HR 7428.

The *HSE* and *NOHSE* best models are shown in Fig. 11 compared with the Solar Val 3c model. We can see that the shape of both the *HSE* and *NOHSE* best models is quite similar to the Solar one. It is worthwhile to notice that the two models describe strongly different geometries. The *HSE* best model describes an atmosphere of the mean K2 primary component of the RS CVn system HR 7428 that extends up to 8×10^5 km, the temperature decreases and reaches the minimum temperature of about 3,000 K at about 500,000 Km above the photosphere, the chromosphere ex-

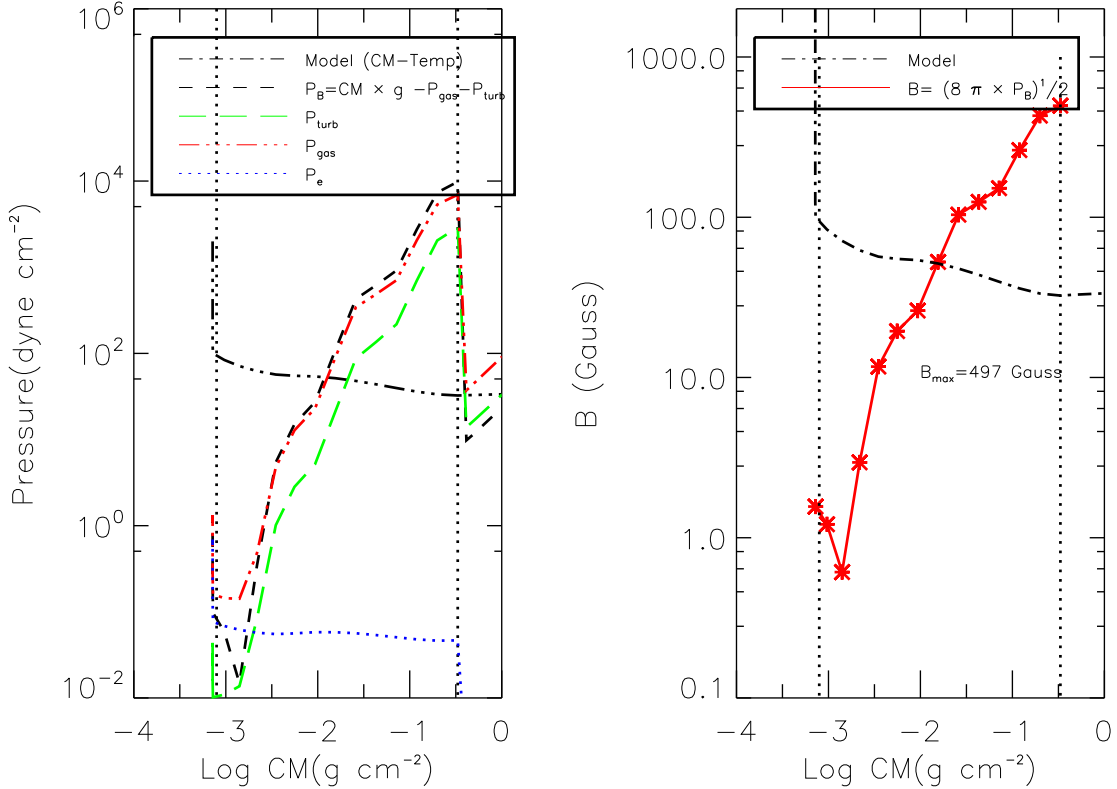


Figure 13. (Left panel:) The new pressure component vs Column Mass is shown (dashed line) in comparison to electron pressure (blue), gas pressure (red), turbulent pressure (green); the atmospheric model is overlapped (dot-dashed line) in order to identify the atmospheric layers where we are comparing the pressure components. (Right panel:) Magnetic field distribution vs Column Mass obtained considering the whole lacking pressure as magnetic pressure.

tends for 250,000 Km from the temperature minimum up to the base of the transition region that is located at about 800,000 Km. The best *NOHSE* models is instead less extended of the *HSE* one; the temperature from the photosphere decreases, reaching the minimum of ≈ 3200 K at about 140,000 Km above the photosphere, the chromosphere extends for 60,000 Km from the temperature minimum up to the base of transition region that is located at about 200,000 Km.

The difference between the *HSE* and the *NOHSE* models can be better understood from the plot of Fig. 12 where the temperature, electron density and total density are plotted versus Column Mass density (CM) defined as P_g for the best *HSE* and *NOHSE* models.

From Fig. 12 panel a), we can see that the *HSE* best model has a minimum of temperature close to 3000 K when the $\log CM \approx -1.04$ and a chromospheric 'plateau' at a temperature of about 6500 K at Column Mass $\approx \log CM = -2$ then temperature rise up to 10,000 K and at $\log CM = -2.25$ we find the base of transition region. In the transition region the temperature rises abruptly up to 200,000 K while the Column Mass remains approximately constant. The *NOHSE* best model has a minimum of temperature ≈ 3250 K (250 K higher with respect to the *HSE* model) at a $\log CM \approx -0.48$ a chromospheric plateau colder than the *HSE* one at about 5500 K and $\log CM = -2.1$. The base of transition region is found here at $\log CM = -3.14$; then temperature rise abruptly up to 200,000 K while the Column Mass remains approximately constant. It is worthwhile to notice (panel b) that in the chromospheric region the *HSE* model presents an electron density rising continu-

ously, while in the *NOHSE* model we observe an abrupt rise of the electron density in a few kilometers while in the main part of the chromosphere the electron density is approximately constant. This result is the same as that found from semi-empirical models of other cool stars (Harper 1992). This abrupt enhancement of electron density corresponds to a density enhancement and to an enhancement of the total pressure. Both in the *HSE* and in the *NOHSE* best models, in the chromospheric layers the density decrease uniformly up to the transition region. Here both electron density and density decrease abruptly.

The most important difference between the two models is shown in Fig. 12 panel d), where the total pressure is plotted versus Column Mass. While, in the *HSE* model, the total chromospheric pressure is imposed to be equal to the Column Mass multiplied for the gravity, that is $P_{Tot} = CM \times g$, and we obtain a straight line, in the *NOHSE* model, the total chromospheric pressure exceed the gravity pressure (dashed line is not a straight line but, in the chromospheric layers lays well above of the gravity pressure).

This exceeding pressure has to be balanced by an equal and opposite pressure otherwise we cannot have a stable star. Therefore, we assumed the difference $P_{Tot} - CM \times g$ as equal, with opposite sign, to the lacking pressure in our calculations, that is: $P_{Totnew} = P_{turb} + P_{gas} + P_{new} = CM \times g$ and therefore $P_{new} = CM \times g - P_{Tot}$.

It is worthwhile to notice that not imposing hydrostatic equilibrium only refers to the chromospheric layers, both the used photospheric and transition regions models were calculated imposing

hydrostatic equilibrium, therefore this new component pressure estimation refers only to this layer.

In Fig. 13 the new pressure component is shown in comparison to electron pressure, gas pressure, turbulent pressure. It is clear that this pressure component is not negligible being of the same order of strength of the gas pressure. In the hypothesis that the additive pressure, could be a magnetic pressure, We calculated a ≈ 500 gauss magnetic field corresponding to a magnetic field that, from the base of the chromosphere decrease toward the outer layers.

5 CONCLUSIONS

We present here the semi-empirical modeling for the K2 star of the RS CVn binary system HR 7428. The model has been computed to match a wide set of observations from the UV continuum to a set of chromospheric lines. The fine coverage in the parameter space used in the modeling let us able to find a good agreement between the observed and computed spectral features. Furthermore a good agreement obtained in matching the UV continuum when use is made of the line-blanketing approximation method of Busá et al. (2001) reinforce the confidence on the method itself.

Although we have obtained an acceptable agreement between the calculations and the observations when the *HSE* is imposed, as it is usual, we do not find an *HSE* model that has a good match with all the used diagnostics. This could be due to many reasons, here we have explored the possibility that we are neglecting some components to the total pressure in the hydrostatic equilibrium equation. Therefore we considered also the radiative transfers without imposing *HSE*. The best model in *NOHSE* gives a much better agreement with observations both in line profiles and in UV continuum. The stability of the best *NOHSE* model, implies the presence of an additive (toward the center of the star) pressure, that decreases in strength from the base of the chromosphere toward the outer layers. Interpreting this additive pressure as a magnetic pressure we estimated a magnetic field intensity of about 500 gauss at the base of the chromosphere.

ACKNOWLEDGEMENTS

We wish to thank the referee, Prof. Donald G. Luttermoser, for his careful reading of the manuscript and for his useful and kind comments and suggestions that we have greatly appreciated. IRAF is distributed by the NOAO which is operated by AURA under contract with NFS.

REFERENCES

- Ayres, T.R., Brown, A., Harper, G.M., Bennett, P.D., Linsky, J.L., Carpenter, K.G., & Robinson, R.D. 1997, ApJ, 491, 876
- Ayres, T.R., Brown, A., & Harper, G.M. 2003, ApJ, 598, 610
- Achmad L., De Jager C., Nieuwenhuijzen H., 1991 A&A 250, 445A
- Andretta V., Busá I., Gomez M.T., Terranegra L., 2005 A&A 430, 669
- Basri, G.S., Linsky, J.L., & Eriksson, K. 1981, ApJ, 251, 162
- Byrne P. B., Abdul Aziz H., Amado P. J., et al., 1998 A&AS 127, 505
- Busá I., Pagano I., Rodonó M., Neff J. E., Lanzafame A. C., 1999 A&A 350, 571B
- Busá I., Andretta V., Gomez M.T., Terranegra L., 2001 A&A 373, 993
- Brown A., Drake S. A., Van Steenberg M. E., Linsky J. L., 1991 ApJ, 373, 614B
- Cardelli J. A., Clayton, G. C., Mathis, J. S., 1989 ApJ, 345, 245C
- Carlsson M., 1986, Technical report 33, Uppsala Astronomical Observatory
- Cram L. E. & Mullan D. J., 1979, ApJ, 234, 579
- Cram L. E. & Mullan D. J., 1979, ApJ, 234, 579
- Fontenla J. M., Avrett E. H., Loeser R. 1993, ApJ 406, 319
- Fontenla, J., White, O.R., Fox, P.A., Avrett, E.H., and Kurucz, R.L. 1999, ApJ, 518, 480
- Gratton L. 1950, ApJ 111, 31
- Griffiths N. W., Jordan C., 1998, ApJ, 497, 883
- Jordan C. & Brown A., 1981 SPSS, 199J
- Hall D. S., Gessner S. E. Lines H. C., Lines R. D., 1990 AJ 100, 2017
- Harper G. M., 1992 MNRAS 256, 37
- Houdebine E. R., 1996 IAU 176, 547H
- Kalkofen W., Ulmschneider, P., Avrett E. H., 1999 ApJ 521, 141
- Kelch, W.L., Linsky, J.L., Basri, G.S., Chiu, H-Y, Chang, S-H, Maran, S.P., & Furenlid, I. 1978, ApJ, 220, 962
- Kurucz R. L. 1993, A new opacity-sampling model atmosphere program for arbitrary abundances, in Peculiar versus normal phenomena in A-type and related stars, IAU Coll. 138, ed. M. M.Dworetzky, F. Castelli, R. Faraggiana, ASP Conf. Ser., 44, 87
- Kurucz R. L., Avrett E.H, 1981, SAOSR, 391, Solar Spectrum Synthesis: A Sample Atlas from 224 to 300 nm
- Lanzafame A. C., Busá I., Rodonó M., 2000, A&A 362, 683
- Leone F., Avila G., Bellassai G., et al., 2016, AJ, 151, 116L
- Linsky J., Redfield S., Ayres T., Brown A., Harper G., 2001, ASPC, 242, 247L
- Luttermoser, D.G., Johnson, H.R., & Eaton, J.A. 1994, ApJ, 422, 351
- Marino G., Catalano S., Frasca A., Marilli E., 2001, A&A 375, 100
- Mauas P. J. D. & Falchi A., 1994, A&A, 281, 129
- Mauas P. J. D., Falchi A., Pasquini L., Pallavicini R., 1997, A&A 326, 249
- Mauas P. J. D., Cacciari C., Pasquini L., 2006, A&A 454, 609
- Pagano I., Ayres T. R., Lanzafame A. C., Linsky J. L., Montesinos B., Rodonó M., 2006 Ap&SS 303,17
- Parsons S. B., Ake T. B. 1987, Bull. Am. Astron. Soc. 19, 708
- Robinson, R.D., Carpenter, K.G., & Brown, A. 1998, ApJ, 503, 396
- Short C. I. & Doyle J. G., 1998, A&A, 336, 613
- Spanó P., Leone F., Bruno P., Catalano S., Martinetti E., Scuderi S., 2006, MSAIS, 9, 481S
- Spanó P., Leone F., Scuderi S., Catalano S., Zerbi F. M., 2004, SPIE, 5492, 373S
- Uitenbroek H., 1992, ASPC, 26, 546
- Vernazza J. E., Avrett E. H., Loeser R., 1973, ApJ 184,605V
- Vernazza J. E., Avrett E. H., Loeser R., 1981, ApJS 45,635
- Vieytes M.; Mauas P.; Cincunegui C., 2005, A&A, 441, 701